Hole transport assisted by the piezoelectric field in $In_{0.4}Ga_{0.6}N$/GaN quantum wells under electrical injection

Shuailong Zhang,[1,2,a,b] Enyuan Xie,[1,a] Tongxing Yan,[3,a] Wei Yang,[3] Johannes Herrnsdof,[1] Zheng Gong,[1,c] Ian M. Watson,[1] Erdan Gu,[1,2,d] Martin D. Dawson,[1] and Xiaodong Hu[3,d]

1. *Institute of Photonics, SUPA, University of Strathclyde, Glasgow G4 0NW, UK*
2. *Joint Laboratory of Advanced Optoelectronic Materials and Devices, State Key Laboratory, Wuhan University of Technology, China and Institute of Photonics, University of Strathclyde, Glasgow G4 0NW, UK*
3. *State Key Laboratory for Artificial Microstructure and Mesoscopic Physics, School of Physics, Peking University, Beijing 100871, China*

a) Shuailong Zhang, Enyuan Xie and Tongxing Yan contributed equally to this work.
b) Current address: School of Engineering, University of Glasgow, G12 8LT, United Kingdom.
c) Current address: mLED Ltd., Glasgow G1 1XN, United Kingdom.
d) Email: erdan.gu@strath.ac.uk; huxd@pku.edu.cn

ABSTRACT:

The authors observe the significant penetration of electrically injected holes through InGaN/GaN quantum wells (QWs) with an indium mole fraction of 40%. This effect and its current density dependence were analysed by studies on micro-pixel light-emitting diodes, which allowed current densities to be varied over a wide range up to 5 kA/cm^2. The systematic changes in electroluminescence spectra, are discussed in the light of the piezoelectric field in the high-indium-content QWs and its screening by the carriers. Simulations were also carried out to clarify the unusual hole transport mechanism and the underlying physics in these high-indium QWs.

I. INTRODUCTION:

InGaN-based light-emitting diodes (LEDs) have the capability to generate light across the whole visible spectrum, making them suitable light sources for a wide range of applications such as solid-state lighting, signalling, displays, and medical applications [1] [2]. The light emitting region in these LEDs is typically an InGaN/GaN multi-quantum-well (MQW) structure where the indium composition of the QWs determines the emission wavelength. However, as the indium content in the InGaN alloy increases above 25%, the quantum efficiency of the LEDs significantly drops, limiting the applications of InGaN LEDs with emission wavelengths longer than 520 nm [3]. The poor quantum efficiency of high-indium content LEDs compared to that of mature blue/green LEDs is mainly due to the strong strain-induced piezoelectric field and the high dislocation/defect density in the LED epitaxial structure [3]-[6].

The carrier transport and distribution mechanism in mature blue/green InGaN LEDs have been systematically studied before, which has been proved to have significant influence on the properties of the devices [7]-[14]. However, there is very little research on the carrier transport and distribution mechanism in InGaN LEDs with indium mole-fractions over 30%. Due to the high-indium content in the active region, such LEDs show many different electrical and optical properties compared with low-indium blue/green InGaN LEDs [3] [15]. Additionally, improvements of the quality of high-indium InGaN/GaN quantum wells (QWs) enabled important demonstrations and applications of LEDs with long emission wavelengths for phosphor-free white lighting, colour-conversion and displays [16]-[19]. Therefore, a clear understanding of the carrier dynamics in high-indium InGaN LEDs can help to optimize the LED epitaxial structure for better device performance and the aforementioned applications.

In this work, we investigated the carrier transport and distribution in an LED structure comprising 7 QWs with 40% indium content and 5 QWs with 18% indium content. In particular, the electroluminescence (EL) of this LED was studied over a wide current density range up to several kA/cm^2. This was enabled by fabricating so-called “micro-LEDs”, i.e. LEDs with typical sizes of several tens of microns or less. Due to a reduction in device self-heating and current crowding, micro-LEDs are able to be driven at very high current densities with very high output power densities, enabling many novel LED applications and the study of LED characteristics in a wide

current density range not accessible using conventional broad-area LEDs [20]-[23]. In this work, it is found that a significant number of holes penetrates through the seven repeat periods of high-indium-content QWs and recombines with electrons in the low-indium-content QWs which are located at the n-side of the junction region. Additionally, we present evidence that the fraction of holes penetrating through the high-indium QWs is dependent on the current density. A finite element simulation indicates that an important factor influencing the hole transport is piezoelectric field which weakens the confining capability of QWs to holes. In this case, the screening of piezoelectric field explains the observed current density dependence.

II. LED WAFER EPITAXIAL GROWTH AND DEVICE FABRICATION

The LED wafer used for micro-LED device fabrication was grown on a *c*-plane sapphire substrate by metal organic chemical vapour deposition. Fig. 1 (a) shows the epitaxial structure of the LED wafer, which consists of a 1.5 μm thick GaN buffer layer, a 4 μm thick n-type GaN layer, a MQW region and a 210 nm thick p-GaN cap layer. The MQW region contains a five-period $In_{0.18}Ga_{0.82}N$ (3 nm)/GaN (10 nm) MQW layer emitting at 460 nm ("bottom QWs"), and a seven-period $In_{0.40}Ga_{0.60}N$ (4 nm)/GaN (13 nm) MQW layer emitting at 600 nm ("main QWs"). More details of the LED wafer, including photoluminescence measurement, can be found in our previous work [5]. Fig. 1 (b) shows a schematic diagram of the conduction energy band without polarization field in the active region of the LED wafer material. The low-indium-content blue QWs function as an electron reservoir for improving the radiative efficiency of the main QWs [24] [25]. More importantly, the main QWs have very high indium mole fraction, inducing 4.27% lattice mismatch between $In_{0.40}Ga_{0.60}N$ and GaN. This large lattice mismatch leads to strong compressive strain in the main QWs, which can result in the generation of defects, dislocations and alloy non-homogeneity [15]. Here, the bottom low indium-content blue QWs may play another beneficial role in partial strain relaxation, thus functioning to optimize the strain distribution and improve the crystal quality of the main QWs [26].

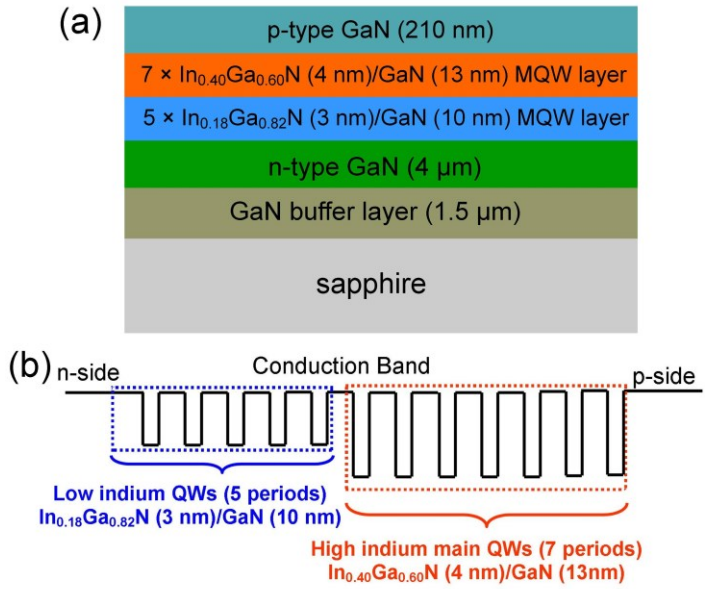

Figure 1: (a) Epitaxial structure of the dual-wavelength high-indium-content LED wafer; (b) schematic diagram of the conduction energy band of the active region of the LED wafer material (without polarisation effect).

The LED wafer was used to fabricate a 10 × 10 array of flip-chip micro-LEDs with 40 μm diameter on a 100 μm pitch. The mesa structure was first etched by Cl_2-based inductively coupled plasma down to the n-type GaN layer. After surface cleaning by a dilute HCl solution, a Ni/Au (10 nm/20 nm) metal bilayer was evaporated on the p-type GaN surface and thermally annealed in an air ambient at 500 ºC to form a semi-transparent metal contact on p-type GaN. The metallization on the n-type GaN was formed by depositing a Ti/Au (50 nm/200 nm) metal bilayer, which filled the area between each micro-LED and enabled an improved current spreading. Then, a 300 nm-thick SiO_2 layer was deposited by plasma-enhanced chemical vapour deposition to isolate each LED element. After selectively removing SiO_2 on top of each micro-LED, another Ti/Au metal bilayer was deposited on top of the oxidized Ni/Au bilayer as a reflector. This bilayer also connects each micro-LED pixel so as to individually address them. Fig. 2 (a) and (b) show a schematic cross-section and the current-voltage (I-V) characteristic of a typical micro-LED pixel from the array, respectively. A microscope image of a section of the array is also shown in the inset of Fig. 2 (b).

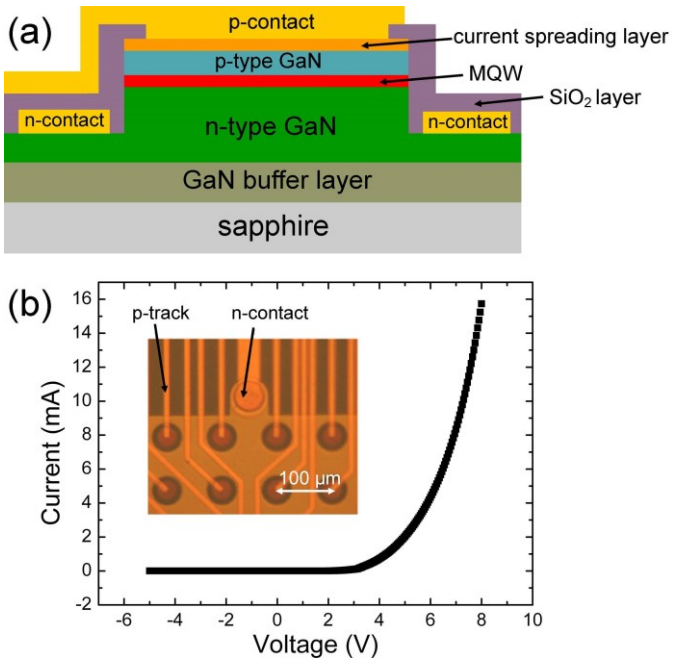

Figure 2: (a) Schematic cross-section and (b) I-V characteristic of a typical 40 µm diameter micro-LED pixel. The inset of (b) shows a microscope image of a section of the micro-LED array device.

III. EXPERIMENTAL RESULTS AND DISCUSSIONS

The EL spectra of the micro-LED device were measured by a fibre-coupled CCD spectrometer (0.1 nm resolution, fibre with 0.22 NA) where the fibre was butt-coupled to the micro-LED. Fig. 3 shows the normalized EL spectra of a typical micro-LED pixel under different injection current densities, taken in pulsed operation (100 µs pulse duration at 0.1 % duty cycle) to minimize thermal effects. Two dominant emission peaks can clearly be seen and are attributed to the main QWs (red-green emission) and the bottom QWs (blue emission). Both evolve differently as a function of injection current density.

The observation of a significant blue emission is surprising because holes have a high effective mass and a low mobility and therefore are a priori not expected to be injected into QWs deeper within the structure [8] [11] [27]-[29]. In previous work on low-indium-content LEDs, both direct observations, such as angle-resolved far-field measurement [8], and indirect indications based on EL spectra have shown that in these structures the QW closest to the p-side of the device has a much higher hole concentration than the other QWs [12]. It was also found that holes are more likely to transport into deep QWs with the increase of injection current [9]. However, as shown

in Fig. 3, the blue emissions in the spectra prove that holes can penetrate through the upper seven-period QWs and recombine in the bottom QWs. The spectra also indicate that such hole penetration and recombination vary with the injection current density. It is important to investigate and understand the physical mechanism responsible for such current-dependent deep hole injection in this LED structure.

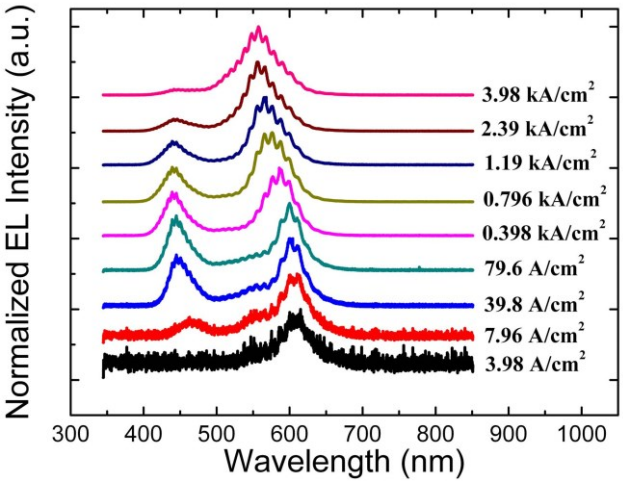

Figure 3: Normalized EL spectra of a typical micro-LED pixel under different injection current densities. The micro-LED pixel is operated under pulsed conditions.

We first discuss the EL spectra in more detail. In order to reduce the influence of detector noise, the measured spectra were fitted by two Gaussian peaks corresponding to main and blue emissions, respectively. Fig. 4 (a) shows the integrated EL intensities of the fitted peaks as a function of injection current density. The intensity of main peak steadily increases with increasing current density similar to that of conventional InGaN LEDs. In contrary, the intensity of the blue peak increases to a peak at around 2-2.3 kA/cm^2 and then drops with further increase of injection current density. Since electrons have a small effective mass and a high mobility, it can be assumed that the intensity of the blue peak reflects the distribution of holes in the device. From 0 to 1 kA/cm^2, there is an intense rise of emission intensity from bottom QWs, indicating that holes can be effectively injected into bottom QWs with the increase of current. From 1 to 3 kA/cm^2, the emission intensity from bottom QWs slightly increases to a peak at around 2-2.3 kA/cm^2 and then slightly decreases. After 3 kA/cm^2, the emission intensity from bottom QWs further drops with the increase of injection current density. Therefore, the hole transport is a current-dependent behaviour. The mechanism which enables the deep hole injection is

weakened with the increase of injection current, causing the drop of the EL emission intensity from the bottom QWs. Fig. 4 (b) shows the integrated EL intensity ratio of the blue peak to main peak. This ratio can be interpreted as a representation of the likelihood of holes to penetrate to the bottom QWs. It can be seen that holes have a significant likelihood to penetrate to the bottom QWs at low injection current densities while at high injection current densities holes are more likely to be trapped in main QWs. Additionally, above 3 kA/cm^2 the intensity ratio is stagnant between 5% and 10%, whereas below 3 kA/cm^2 it varies strongly and a sharp drop of the intensity ratio can be clearly viewed.

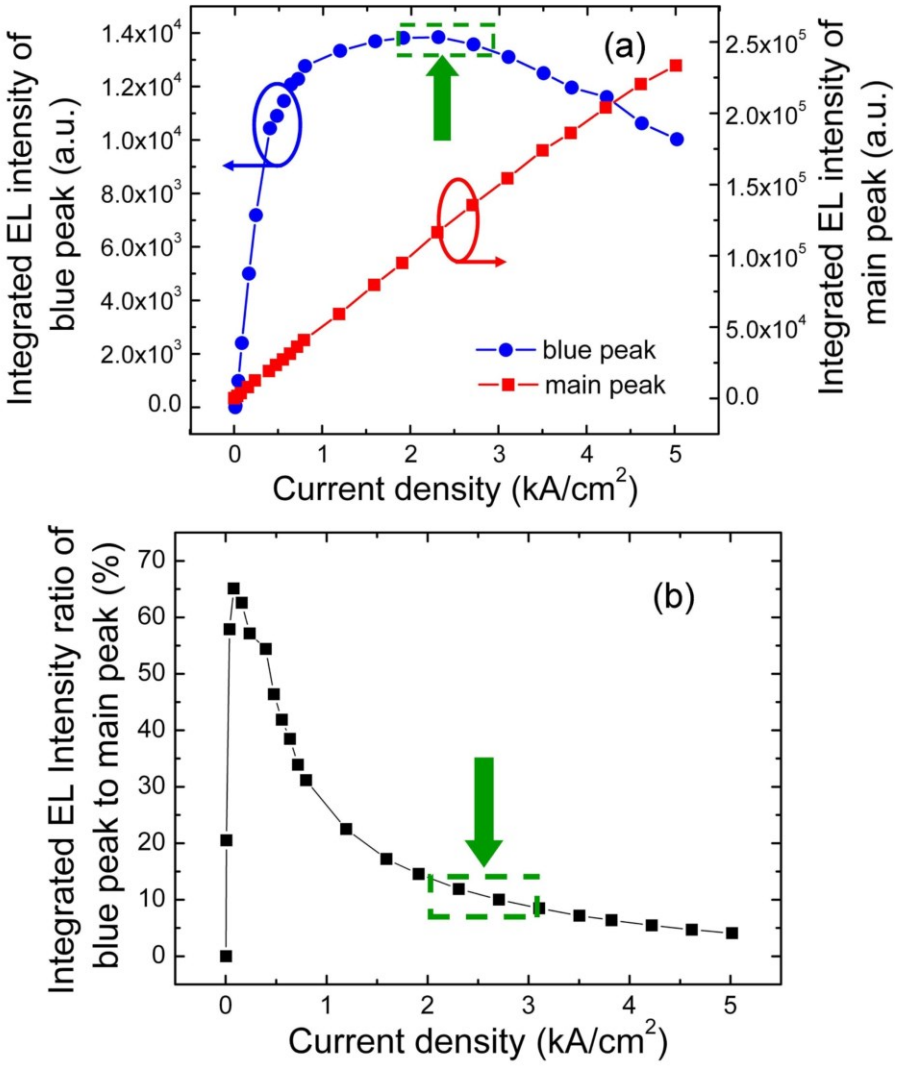

Figure 4: (a) Integrated EL intensity of the fitted two peaks (blue peak and main peak) from a typical micro-LED pixel under different injection current densities; (b) integrated EL intensity ratio of blue peak to main peak. The micro-LED pixel is operated under pulsed conditions.

We now explore the physical mechanisms controlling the hole distributions in the QWs with different indium-contents. In the device discussed here, the piezoelectric field in the main QWs has an important influence on the device performance and is also a likely reason for the hole penetration [15]. In general, the strong piezoelectric field and the current-dependent screening of the piezoelectric field have a big influence on the band structure of QWs and thus the carrier dynamics [15], [30]. In other words, the piezoelectric polarization due to lattice mismatch induces a build-in electric field in the polar QW, known as the piezoelectric field. This piezoelectric field can be screened by the injection carriers, which has a big influence on the band structure of QWs and thus the carrier dynamics [5]. The influence of the piezoelectric effect can be seen in the spectra shown in Fig. 3. At low current densities the main QW emission peak occurs at the target wavelength of 600 nm. However, with the increase of current density, it blue-shifts to 550 nm which is mainly due to two reasons, i.e. the screening of piezoelectric field (also known as the screening of quantum confined Stark effect) and the band-filling effect [5],[31]-[34]. However, the screening of piezoelectric field induces the narrowing of the emission spectra due to the flat energy band and enhanced overlap of electron and hole wave functions [35],[36]. While the band-filling effect induces the broadening of the emission spectra [37]. Shown in Fig. 5 are the corresponding peak position and full width at half maximum (FWHM) of the main peak extracted from the Gaussian fit. It can be seen that, in the current density range from 0 to 3 kA/cm^2, there is a sharp blue-shift (about 50 nm) of the peak position accompanied by a narrowing of the FWHM. This indicates that, in this current density range, the blue-shift of the main emission peak is dominated by the screening effect of the piezoelectric field by injection carriers. Above 3 kA/cm^2, the FWHM increases associated with a slight blue-shift of the peak position. In this regime, band-filling is likely the main driver for the broadening of FWHM and the slight blue-shift. This interpretation is in good agreement with our previous simulation results as the piezoelectric field is mostly screened above 3 kA/cm^2 [5]. Therefore, the dominant factor determining the spectral behaviour changes at a current density regime of 2-3 kA/cm^2, as indicated by the green arrow and dashed box in Fig. 5. Interestingly, this current density regime also matches very well with the current density regime highlighted by the green arrow and dashed box in Fig. 4 (a) and (b), where the emission intensity of blue QWs reaches its maximum value and the sharp drop of the integrated EL ratio stops. This coincidence

is an indication that the hole penetration below 3 kA/cm^2 is dominated by the piezoelectric field in the QWs.

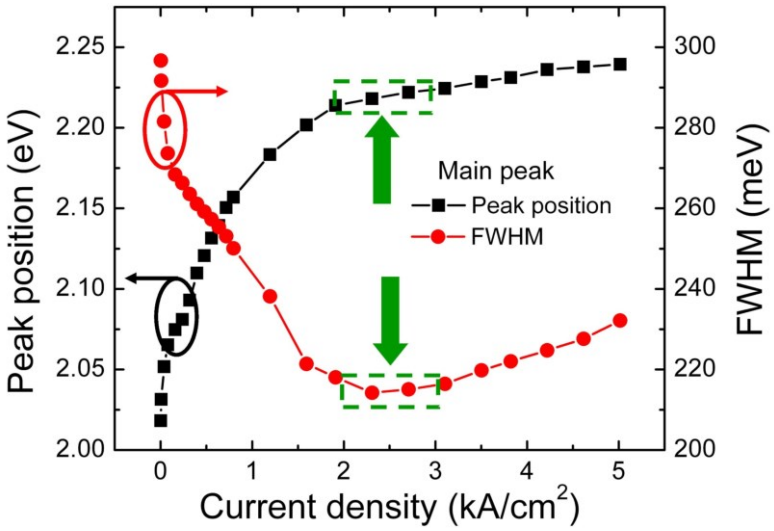

Figure 5: Peak position and corresponded FWHM of the main emission peak of a micro-LED pixel as a function of pulsed operating current.

This phenomenon can be interpreted as follows. A strong piezoelectric field severely tilts the band structure of QWs, decreasing the effective width of QW and subsequently leading to a strong flyover of carriers across the QW and a decrease of carrier capture rate of the QWs [15], [30]. Additionally, the ground state energy of electrons or holes in the narrow and tilted well is higher than that in the wider and standard well [15], [38], thus increasing the carrier escape rate. Also, the reduced overlap of hole and electron wave functions in a QW with piezoelectric field [7] results in a longer carrier lifetime and thus increases the chance of carrier escape. The schematics shown in Fig. 6 (a) and (b) illustrate these relevant factors on the carrier capture process and the energy state in a QW with and without piezoelectric field. As shown, the piezoelectric field can promote the transport of holes into deeper QWs while the screening of piezoelectric field can increase the confining capability of QWs, suppressing the transport of holes. It is probably for this reason that the emission from bottom QWs increases to a peak at around 2-2.3 kA/cm^2 and decreases at higher current densities. Additionally, the sharp drop of integrated intensity ratio shown in Fig. 4 (b) appears in the current density regime (before 3 kA/cm^2) where there is a strong screening of piezoelectric field ongoing and the stagnant of integrated intensity ratio appears in the current density regime (after 3 kA/cm^2) where the piezoelectric

field is severely minimized. In Fig.4, when the current increases in a range from 0 to 0.079 kA/cm2, the light intensity of bottom quantum wells increases relatively more significant than the light intensity of main quantum wells, inducing an increase of the ratio. This phenomenon has not been fully understood and is still under investigation. A possible reason is that the piezoelectric field in the bottom quantum wells is smaller than that in the main quantum wells. The smaller piezoelectric field in the bottom quantum wells is due to their lower indium mole fraction and corresponding smaller distribution of compressive strain. Details of the smaller piezoelectric field in bottom quantum wells, including experimental and simulation results, can be found in our previous work [5]. Therefore, the screening effect of carriers to piezoelectric field is relatively stronger than that in the main quantum wells under low injection current density and the light intensity of bottom quantum wells may increase relatively more significant than the light intensity of main quantum wells, inducing the increase of the ratio at low injection current density.

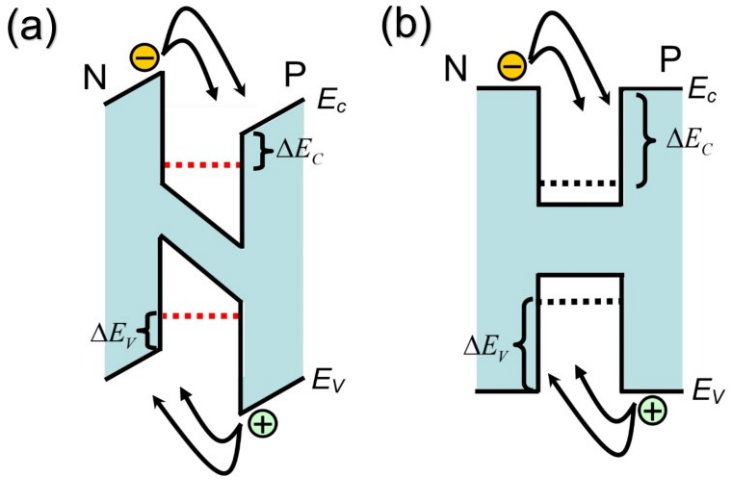

Figure 6: Carrier capture process and schematic band diagram of an InGaN/GaN QW (a) with and (b) without piezoelectric field. Since the LED wafer was grown on *c*-plane sapphire substrate and the compressive strain exists in the QW (InGaN on top of GaN), the direction of piezoelectric field is from right hand side (P-GaN side) to left hand side (N-GaN side).

In order to provide further insight on the influence of the piezoelectric field on hole transport mechanism in this dual-wavelength LED, simulations were carried out based on an advanced self-consistent k.p model embedded in a commercial simulation software APSYS [39]-[41]. This software couples Poisson equation, Schrödinger

equation in quantum well (by 6×6 band k.p theory for valence band and 2×2 effective mass approximation for conduction band [41]), electron and hole current continuity equation and LED ray-tracing equation. All equations were numerically solved simultaneously by finite difference scheme with no-prior settings. More details of the self-consistent k.p model and the simulation method can be found elsewhere [42]-[46]. The simulation in this work was based on the LED structure described in Section II, except that a simple two set QWs were adopted: a low-indium-content ($In_{0.18}Ga_{0.82}N$) QW layer (3 nm)/GaN (10 nm) and a high-indium-content ($In_{0.40}Ga_{0.60}N$) QW layer (4 nm)/GaN (13 nm). This simplification gives rapid convergence for simulation with reasonable computation time, and at the same time does not hinder to reveal the physical mechanism of our dual-wavelength LED structure. To demonstrate the influence of piezoelectric field and the screening of piezoelectric field, two simulation runs were performed: one with interface charge, which is automatically set by the software according to indium composition; another one without interface charge, which is manually set to zero. The simulation run with interface charge was used to represent the practical case where there is a strong piezoelectric field existing in the high-indium-content QW; while the simulation run without interface charge was used to represent an ideal case that the piezoelectric field is screened. In this way, the comparison of the QW with and without piezoelectric field can be made [47] [48]. It is worth noting that the setting of interface charge in the simulation is equivalent to that of piezoelectric field or polarization dipole moment [49]. 50% interface charge (0.5 screening ratio) were adopted in the simulation run with interface charge due to a weaker built-in polarization found in actual experiments [50],[51], which in our case gives an interface charge density of $1.5\times10^{13}/cm^2$ for the high-indium-content QW. This screening ratio only represents the screening of doping and defects to piezoelectric field [52]. All other material parameters used are from literature [53] and were kept the same for the two runs.

Fig. 7 shows the energy band diagrams and quasi-Fermi levels of the QWs with and without piezoelectric field. The injection current density is 500 A/cm^2. As shown in Fig. 7 (a), in the valence band of the QWs without piezoelectric field, the quasi-Fermi level is well above the band edge of the low-indium-content QW, which indicates that very few holes can be injected into this QW. In contrast, in the valence band of the QWs with piezoelectric field (Fig. 7 (b)), the quasi-Fermi level overlaps the band edge of the low-indium-content QW, which indicates that holes can be

injected into this QW. In Fig. 7 (b), the band bending of p-side does not arise significantly nearby the interface between p-side and QW, which is mainly due to two reasons. Firstly, Fig. 7 (b) is plotted at an injection current density of 500 A/cm^2, applying such injection current density associated with high bias would flatten the band structure. Secondly, our structure does not have an AlGaN electron blocking layer. Therefore, the piezoelectric polarization mismatch between the QW and p-type GaN is small. Fig. 8 shows the hole density of the QWs with and without piezoelectric field under an injection current density of 500 A/cm^2. As shown, the hole density in the low-indium-content QW with piezoelectric field is an order of magnitude higher than that without piezoelectric field. In addition, the hole density ratio of low-indium-content QW to high-indium-content QW increases substantially when the piezoelectric field is applied. These simulation results match up well with the experimental results and prove that the piezoelectric field promotes the penetration of holes into deeper QWs. For QW with different Indium composition, the piezoelectric field and the screening effect of carriers also exist. Therefore, the reason of the hole penetration discussed in this work should play an role as well. However, the intensity of piezoelectric field and its screening by carriers in the QW varies strongly with different Indium composition. Our results show what happens in an extreme case of high indium composition and the exact dependence of the effect on the indium composition will be studied in the future.

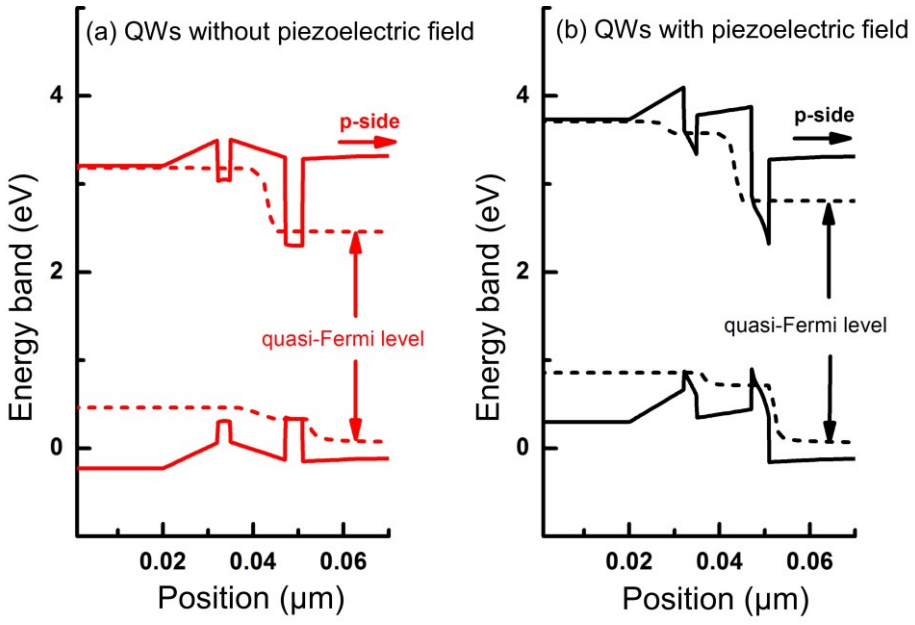

Figure 7: Energy band diagrams of QWs (a) without piezoelectric field and (b) with piezoelectric field under an injection current density of 500 A/cm^2.

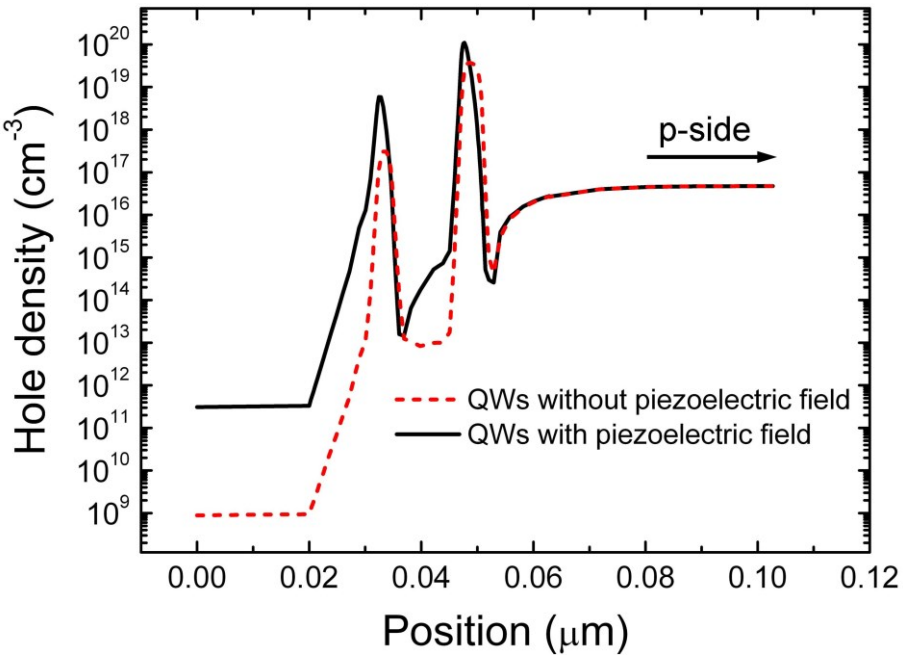

Figure 8: Hole concentrations of the QWs with and without piezoelectric field under an injection current density of 500 A/cm^2.

IV. CONCLUSION:

In summary, we have investigated the effect of hole penetration through a number of high-indium-content QWs in an InGaN micro-LED. It is demonstrated that the hole transport mechanism in this structure depends on the current density and coincides with screening of the built-in piezoelectric field. Studies on micro-LEDs allowed the current density to be varied over a wide range, up to 5 kA/ cm^2. Based on the EL spectra, it is discussed how the piezoelectric field and its screening can indeed explain the observed behaviour of the device. Furthermore, this view is underpinned by simulation results which show that the piezoelectric field can increase the capability of hole transport into deeper QWs. Therefore, by investigating the carrier transport and distribution, this research provides insight into the piezoelectric field related mechanism underlying the current-dependent EL spectra observed in the high-indium-content InGaN micro-LED device.

ACKNOWLEDGMENTS

This work was supported by the Engineering and Physical Sciences Research Council through HYPIX Project under Grant EP/F05999X/1 and Ultra-parallel Visible Light Communications Project under Grant UP-VLC EP/K00042X/1.

REFERNCE

[1] E. F. Schubert and J. K. Kim, "Solid-State Light Sources Getting Smart", *Science,* **308**, 1274 (2005).

[2] S. Pimputkar, J. S. Speck, S. P. DenBaars, and S. Nakamura, "Prospects for LED lighting", *Nat. Photon.*, **3**, 180 (2009).

[3] T. Mukai, M. Yamada, and S. Nakamura, "Characteristics of InGaN-based UV/blue/green/amber/red light-emitting diodes", *Jap. J. Appl. Phys.*, **38**, 3976, (1999).

[4] J.-I. Hwang, R. Hashimoto, S. Saito, and S. Nunoue, "Development of InGaN-based red LED grown on (0001) polar surface", *Appl. Phys. Exp.,* **7**, 071003 (2014).

[5] Z. Gong, N. Y. Liu, Y. B. Tao, D. Massoubre, E. Y. Xie, X. D. Hu, Z. Z. Chen, G. Y. Zhang, Y. B. Pan, M. S. Hao, I. M.Watson, E. Gu, and M. D. Dawson, "Electrical, spectral and optical performance of yellow–green and amber micro-pixelated InGaN light-emitting diodes", *Semicond. Sci. Technol.*, **27**, 015003 (2012).

[6] H.-S. Chen, C.-F. Lu, D.-M. Yeh, C.-F. Huang, J.-J. Huang, and C.-C. Yang, "Orange–red light-emitting diodes based on a prestrained InGaN–GaN quantum-well epitaxy structure", *IEEE Photon. Technol. Lett.,* **18**, 2269 (2006).

[7] R. Charash, P. P. Maaskant, L. Lewis, C. McAleese, M. J. Kappers, C. J. Humphreys, and B. Corbett, "Carrier distribution in InGaN/GaN tricolor multiple quantum well light emitting diodes", *Appl. Phys. Lett.,* **95**, 151103 (2009).

[8] A. l. David, M. J. Grundmann, J. F. Kaeding, N. F. Gardner, T. G. Mihopoulos, and M. R. Krames, "Carrier distribution in (0001)InGaN ⁄ GaN multiple quantum well light-emitting diodes," *Appl. Phys. Lett.,* **92,** 053502 (2008).

[9] M. Meneghini, S. Vaccari, A. Garbujo, N. Trivellin, D. Zhu, C. J. Humphreys, M. Calciati, M. Goano, F. Bertazzi, G. Ghione, E. Bellotti, G. Meneghesso, and E. Zanoni, "Electroluminescence Analysis and Simulation of the Effects of Injection and Temperature on Carrier Distribution in InGaN-Based Light-Emitting Diodes with Color-Coded Quantum Wells", *Jap. J. Appl. Phys.,* **52**, 08JG09 (2013).

[10] T. S. Kim, B. J. Ahn, Y. Dong, K. N. Park, J. G. Lee, Y. Moon, H. K. Yuh, S. C. Choi, J. H. Lee, S. K. Hong, and J. H. Song, "Well-to-well non-uniformity in InGaN/GaN multiple quantum wells characterized by capacitance-voltage measurement with additional laser illumination", *Appl. Phys. Lett.,* **100**, 071910 (2012).

[11] J. Cho, E. F. Schubert, and J. K. Kim, "Efficiency droop in light-emitting diodes: Challenges and countermeasures", *Laser Photon. Rev.,* **7**, 408 (2013).

[12] J. P. Liu, J. H. Ryou, R. D. Dupuis, J. Han, G. D. Shen, and H. B. Wang, "Barrier effect on hole transport and carrier distribution in InGaN / GaN multiple quantum well visible light-emitting diodes", *Appl. Phys. Lett.,* **93**, 021102 (2008).

[13] J.-Y. Zhang, L.-E. Cai, B.-P. Zhang, X.-L. Hu, F. Jiang, J.-Z. Yu, Q.-M. Wang, "Efficient hole transport in asymmetric coupled InGaN multiple quantum wells", *Appl. Phys. Lett.,* **95**, 161110 (2009).

[14] Z. Zheng, Z. Chen, Y. Chen, H. Wu, S. Huang, B. Fan, Z. Wu, G. Wang and H. Jiang, "Improved carrier injection and efficiency droop in InGaN/GaN light-emitting diodes with step-stage multiple-quantum-well structure and hole-blocking barriers", *Appl. Phys. Lett.*, **102**, 241108 (2013).

[15] E. F. Schubert. Light-emitting diodes. Cambridge University Press, second edition, 2008.

[16] M. Yamada, Y. Narukawa, and T. Mukai, "Phosphor Free High-Luminous-Efficiency White Light-Emitting Diodes Composed of InGaN Multi-Quantum Well", *Jap. J. Appl. Phys.,* **41**, 246 (2002).

[17] Y. J. Hong, C.-H. Lee, A. Yoon, M. Kim, H.-K. Seong, H. J. Chung, C. Sone, Y. J. Park, and G.-C. Yi, "Visible-Color-Tunable Light-Emitting Diodes", *Adv. Mater.,* **23**, 3284 (2011).

[18] B. Damilano, H. K.-Chauveau, E. Frayssinet, J. Brault, S. Hussain, K. Lekhal, P. Vennegues, P. D. Mierry, and J. Massies, "Metal Organic Vapor Phase Epitaxy of Monolithic Two-Color Light-Emitting Diodes Using an InGaN-Based Light Converter", *Appl. Phys. Exp.,* **6**, 092105 (2013).

[19] S. Zhang, Z. Gong, J. J. D. McKendry, S. Watson, A. Cogman, E. Xie, P. Tian, E. Gu, Z. Chen, G. Zhang, A. E. Kelly, R. K. Henderson, M. D. Dawson, "CMOS-Controlled Color-Tunable Smart Display", *IEEE Photon. J.,* **4**, 1639 (2012).

[20] Z. Y. Fan, J. Y. Lin, and H. X. Jiang, "III-nitride micro-emitter arrays: development and applications", *J. Phys. D: Appl. Phys.,* **41**, 094001 (2008).

[21] H. X. Jiang and J. Y. Lin, "Nitride micro-LEDs and beyond - a decade progress review", *Opt. Exp.,* **21**, A475 (2013).

[22] Z. Gong, S. Jin, Y. Chen, J. McKendry, D. Massoubre, I. M. Watson, E. Gu, and M. D. Dawson, "Size-dependent light output, spectral shift, and self-heating of 400 nm InGaN light-emitting diodes", *J. Appl. Phys.,* **107**, 013103 (2010).

[23] W. Yang, S. Zhang, J. J. D. McKendry, J. Herrnsdorf, P. Tian, Z. Gong, Q. Ji, I. M. Watson, E. Gu, M. D. Dawson, L. Feng, C. Wang, and X. Hu, "Size dependent capacitance study on InGaN-based micro-light-emitting diodes", *J. Appl. Phys.,* **116**, 044512 (2014).

[24] N. Otsuji, K. Fujiwara, and J. K. Sheu, "Electroluminescence efficiency of blue InGaN / GaN quantum-well diodes with and without an n-InGaN electron reservoir layer", *J. Appl. Phys.,* **100**, 113105 (2006).

[25] X. Ni, X. Li, J. Lee, S. Liu, V. Avrutin, U. Özgür, H. Morkoç, A. Matulionis, T. Paskova, G. Mulholland, and K. R. Evans, "InGaN staircase electron injector for reduction of electron overflow in InGaN light emitting diodes", *Appl. Phys. Lett.,* **97**, 031110 (2010).

[26] W.-Y. Shiao, C.-F. Huang, T.-Y. Tang, J.-J. Huang, Y.-C. Lu, C.-Y. Chen, Y.-S. Chen, and C. C. Yang, "X-ray diffraction study on an InGaN / GaN quantum-well structure of prestrained growth", *J. Appl. Phys.,* **101**, 113503 (2007).

[27] D. S. Meyaard, G.-B. Lin, Q. Shan, J. Cho, E. Fred Schubert, H. Shim, M.-H. Kim, and C. Sone, "Asymmetry of carrier transport leading to efficiency droop in GaInN based light-emitting diodes", *Appl. Phys. Lett.,* **99**, 251115 (2011).

[28] X. Ni, Q. Fan, R. Shimada, U. m. Özgür, and H. Morkoç, "Reduction of efficiency droop in InGaN light emitting diodes by coupled quantum wells", *Appl. Phys. Lett.,* **93**, 171113 (2008).

[29] C. H. Wang, J. R. Chen, C. H. Chiu, H. C. Kuo, Y-L. Li, T. C. Lu, and S. C. Wang, "Temperature-dependent electroluminescence efficiency in blue InGaN–GaN light-emitting diodes with different well widths", *IEEE Photon. Technol. Lett.*, **22**, 236, (2010).

[30] M. F. Schubert and E. F. Schubert, "Effect of heterointerface polarization charges and well width upon capture and dwell time for electrons and holes above GaInN/GaN quantum wells", *Appl. Phys. Lett.,* **96**, 131102 (2010).

[31] C.-H. Chen, S.-J. Chang and Y.-K. SU, "High-Indium-Content InGaN/GaN Multiple-Quantum-Well Light-Emitting Diodes", *Jap. J. Appl. Phys.,* **42**, 2281 (2003).

[32] M.-J. Lai, M.-J. Jeng, and L.-B. Chang, "High-Efficiency InGaN-Based Yellow-Green Light-Emitting Diodes", *Jap. J. Appl. Phys.,* **49**, 021004 (2010).

[33] T. Takeuchi, C.Wetzel, S. Yamaguchi, H. Sakai, H. Amano, I. Akasaki, Y. Kaneko, S. Nakagawa, Y. Yamaoka, and N. Yamada, "Determination of piezoelectric fields in strained GaInN quantum wells using the quantum-confined Stark effect", *Appl. Phys. Lett.,* **73**, 1691 (1998).

[34] J.-H. Ryou, P. D. Yoder, J. Liu, Z. Lochner, H. Kim, S. Choi, H. J. Kim, and R. D. Dupuis, "Control of quantum-confined stark effect in InGaN-based quantum wells," *IEEE J. Sel. Top. Quant. Electron.*, **15**, 1080 (2009).

[35] Y.-J. Lee, C.-H. Chiu, C. C. Ke , P. C. Lin, T.-C. Lu, H.-C. Kuo, and S.-C. Wang, "Study of the excitation power dependent internal quantum efficiency in InGaN/GaN LEDs grown on patterned sapphire substrate," *IEEE J. Sel. Top. Quantum Electron.*, **15**, 1137 (2009).

[36] J.-H. Chen, Z.-C. Feng, H.-L. Tsai, J.-R. Yang, P. Li, C. Wetzel, T. Detchprohm and J. Nelson, "Optical and structural properties of InGaN/GaN multiple quantum well structure grown by metalorganic chemical vapor deposition," *Thin Solid Films*, **498**, 123 (2006).

[37] Y. D. Qi, H. Liang, D. Wang, Z. D. Lu, W. Tang, and K. M. Lau, "Comparison of blue and green InGaN/GaN multiple-quantum-well light-emitting diodes grown by metalorganic vapor phase epitaxy," *Appl. Phys. Lett.,* **86**, 101903 (2005).

[38] J.-Y. Zhang, L.-E. Cai, B.-P. Zhang, X.-L. Hu, F. Jiang, J.-Z. Yu, Q.-M. Wang, "Efficient hole transport in asymmetric coupled InGaN multiple quantum wells", *Appl. Phys. Lett.,* **95**, 161110 (2009).

[39] APSYS, Version 2008.06.01, Crosslight Software, Inc., Burnaby Canada, 1995–2005.

[40] Z.-M. Li, K. M. Dzurko, A. Delage, and S. P. McAlister, "A self-consistent two-dimensional model of quantum-well semiconductor lasers: optimization of a GRIN-SCH SQW laser structure", *IEEE J. Quant. Electron.*, **28**, 792 (1992).

[41] S. L. Chuang, and C. S. Chang, "A band-structure model of strained quantum-well wurtzite semiconductors," *Semicond. Sci. Technol.*, **12**, 252 (1997).

[42] L. Liu, L. Wang, N. Liu, W. Yang, D. Li, W. Chen, Z. C. Feng, Y. C. L, I. Ferguson, and X. Hu, "Investigation of the light emission properties and

carrier dynamics in dual-wavelength InGaN/GaN multiple-quantum well light emitting diodes", *J. Appl. Phys.*, **112**, 083101 (2012).

[43] W. Yang, D. Li, N. Liu, Z. Chen, L. Wang, L. Liu, L. Li, C. Wan, W. Chen, X. Hu, and W. Du, "Improvement of hole injection and electron overflow by a tapered AlGaN electron blocking layer in InGaN-based blue laser diodes", *Appl. Phys. Lett.*, **100**, 031105 (2012).

[44] M. Gladysiewicz, R. Kudrawiec, and M. S. Wartak, "Electronic Band Structure and Material Gain of Dilute Nitride Quantum Wells Grown on InP Substrate", *IEEE J. Quant. Electron.*, **51**, 7100212 (2015).

[45] B. Chen, W. Y. Jiang, and A. L. Holmes Jr., "Design of strain compensated InGaAs/GaAsSb type-II quantum well structures for mid-infrared photodiodes", *Opt. Quant. Electron.*, **44**,103 (2012).

[46] B. Chen and A. L. Holmes Jr., "Optical gain modeling of InP based InGaAs(N)/GaAsSb type-II quantum wells laser for mid-infrared emission", *Opt. Quant. Electron.*, **45**, 127 (2013).

[47] Z. Yang, R. Li, Q. Wei, T. Yu, Y. Zhang, W. Chen, and X. Hu, "Analysis of optical gain property in the InGaN/GaN triangular shaped quantum well under the piezoelectric field", *Appl. Phys. Lett.*, **94**, 061120 (2009).

[48] J.-R. Chen, C.-H. Lee, T.-S. Ko, Y.-A. Chang, T.-C. Lu, H.-C. Kuo, Y.-K. Kuo, and S.-C. Wang, "Effects of built-in polarization and carrier overflow on InGaN quantum-well lasers with electronic blocking layers", *J. Lightwave Technol.*, **26**, 329 (2008).

[49] F. Bernardini and V. Fiorentini, "Nonlinear macroscopic polarization in III-V nitride alloys", *Phys. Rev. B,* **64**, 085207 (2001).

[50] J. P. Ibbetson, P. T. Fini, K. D. Ness, S. P. DenBaars, J. S. Speck, and U. K. Mishra, "Polarization effects, surface states, and the source of electrons in AlGaN/GaN heterostructure field effect transistors", *Appl. Phys. Lett.*, **77**, 250 (2000).

[51] S. F. Chichibu, A. C. Abare, M. S. Minsky, S. Keller, S. B. Fleischer, J. E. Bowers, E. Hu, U. K. Mishra, L. A. Coldren, S. P. DenBaars, and T. Sota, "Effective band gap inhomogeneity and piezoelectric field in InGaN/GaN multiquantum well structures ", *Appl. Phys. Lett.*, **73**, 2006 (1998).

[52] Y.-K. Kuo, M.-C. Tsai, S.-H. Yen, T.-C. Hsu, and Y.-J. Shen, "Enhancement of Light Power for Blue InGaN LEDs by Using Low-Indium-Content InGaN Barriers", *IEEE J. Sel. Top. Quant. Electron.*, **15**, 1115 (2009).

[53] I. Vurgaftman and J. R. Meyer, "Band parameters for nitrogen-containing semiconductors ", *J. Appl. Phys.*, **94**, 3675 (2003).

The relation between k.p theory, self-consistent k.p theory and device simulation models:

1. Device simulation models:

The basic equations to describe the electrical behavior of device are the following:

a) Poisson's equation of electric potential V (field)

$$-\nabla\cdot(\varepsilon\varepsilon_0\nabla V) = -n + p + N_D(1-f_D) - N_A f_A + \sum_j N_{tj}(\delta_j - f_{tj}) + N_{it},$$

$$E = -\nabla V$$

n, p: electron and hole concentration, usually by injection;

N_D, N_A: donor and acceptor concentration;

N_{tj}: defect density for deep trap of j level;

N_{it}: interface charge density, for example, polarization charge.

b) Current continuity equations for electrons and holes

$$\nabla\cdot\frac{1}{q}J_n = \sum_j U_{tj} - R_{sp} - R_{st} - R_{auger} + G_{opt}(t) = \frac{\partial n}{\partial t} + N_D\frac{\partial f_D}{\partial t}$$

$$\nabla\cdot\frac{1}{q}J_p = \sum_j U_{tj} + R_{sp} + R_{st} + R_{auger} - G_{opt}(t) = -\frac{\partial p}{\partial t} + N_A\frac{\partial f_A}{\partial t}$$

The basic equations to describe optical behavior are:

c) Wave equation for light:

$$\nabla^2 W(x,y) + k_0^2(\varepsilon(x,y) - \beta^2)W(x,y) = 0$$

d) Photon rate equation

$$\frac{c}{\beta_1}[g_m - \frac{1}{2L}\ln(\frac{1}{r_m})]S + c_m\int R_{sp}dv = 0$$

For light emitting devices, light output power (LOP) is very important. Basically, $LOP \propto R_{sp}$, where R_{sp} is the spontaneous recombination term. In a simple ABC model based on classical theory, $R_{sp} = Bn^2$, but it usually requires quantum mechanical

calculation of band structure in quantum wells (this is exactly what have been done in our simulation by k.p theory).

2. k.p theory:

k.p theory is a way to solve the Schrödinger equation in semiconductors to obtain band structure, wave function and recombination terms. It is a very old topic, while k.p theory for nitride was recently developed by S. L. Chuang. The k.p theory for nitride devices is slightly different from that for GaAs-based ones. One key issue is how to deal with polarization field, which was represented by the method by Bernardini, F. and V. Fiorentini (F. Bernardini and V. Fiorentini, "Nonlinear macroscopic polarization in III-V nitride alloys," Physics Review B, Vol. 64, No. 8, pp. 085207 (2001)).

3. Self-consistent k.p theory

The self-consistent k.p theory just means a simultaneous solution of Schrödinger equation and Poisson equation. So our model is in nature a self-consistent k.p theory incorporated with more advanced models for nitride devices.

4. The methodology of using no polarization field as a reference in polar QWs

The methodology of using no polarization field as a reference in polar QWs has been accepted in many groups in the GaN community. Here give some researchers and references:

[1] Joachim Piprek, Robert Farrell, Steve DenBarrs, and Shuji Nakamura, "Effects of built-in polarization on InGaN-GaN vertical-cavity surface-emitting lasers", *IEEE Photonics Technology Letters*, Vol. 18, No. 1, pp.7-9, 2006.

[2] Jun-Rong Chen, Chung-Hsien Lee, Tsung-Shine Ko, Yi-An Chang, Tien-Chang Lu, Hao-Chung Kuo, Yen-Kuang Kuo, and Shing-Chung Wang, "Effects of built-in polarization and carrier overflow on InGaN quantum-well lasers with electronic

blocking layers", *Journal of Lightwave Technology*, Vol. 26, No. 3, pp.329-337, 2008.

[3] Ziwen Yang, Rui Li, Qiyuan Wei, Tao Yu, Yanzhao Zhang, Weihua Chen, and Xiaodong Hu, "Analysis of optical gain property in the InGaN/GaN triangular shaped quantum well under the piezoelectric field," *Applied Physics Letters*, Vol. 94, No. 6, pp.061120, 2009.

5. Polarization charge, polarization field and screen effect

Polarization field includes piezoelectric polarization and also spontaneous polarization. Polarization field was equivalent to interface charges through Poisson equation:

$$\frac{\varepsilon_0 \varepsilon_{dc}}{q} \nabla \square = \cdot\cdot$$

N_{it} stands for polarization charge at the interface. As there are defects, deep level traps, donor and acceptor (as shallow level traps) in the material. Even at zero bias where there is no current injection, the field is still screened. Therefore, the equation changes to:

$$\frac{\varepsilon_0 \varepsilon_{dc}}{q} \nabla \square = \cdot\cdot \quad \int_{defects},$$

According to experiment, the screen ratio is 20%-80%, and we set it at 50% in our work. Note that N_{it} and $N_{defects}$ generally do not move in the material and also do not change with current injection (so the screen ratio is relatively unchanged), that is

$$N_{it} = N_0 \delta(\mathrm{x} - \mathrm{x}_{it}), \forall j$$

When current density increases, free carriers such as electrons and holes increases, which can be calculated by current continuity equation:

$$\nabla \square \cdot\cdot \quad \frac{\overline{\quad}}{\underline{\quad}} \; {}^{tj}_{n} - R_{sp} - R_{st} - R_{auger} + G_{opt}(t) = \frac{\partial n}{\partial t} + N_D \frac{\partial f_D}{\partial t}$$

In the steady state, electron or hole concentration is a function of space variable and current density *n(x,j)*. Because there exists the field, we have

$$n(\mathrm{x},\mathrm{j}) \neq p(\mathrm{x},\mathrm{j}), \forall \mathrm{x}$$

Instead

$$\sum_x n(\mathrm{x},\mathrm{j}) = \sum_x p(\mathrm{x},\mathrm{j}), \forall j$$

Above is the charge neutrality condition in the device. So now the Poission equation is

$$\frac{\varepsilon_0 \varepsilon_{dc}}{q} \nabla \square = \; .. \quad \sqrt{}_{defects} \text{-}n(x,j) + p(x,j),$$

We see how the screen ratio changes with current injection.

$$\frac{\varepsilon_0 \varepsilon_{dc}}{q} \nabla \square \quad .. \xrightarrow{\text{screened by defects,deep/shallow level traps}}$$

$$\frac{\varepsilon_0 \varepsilon_{dc}}{q} \nabla \square \quad .. \quad \sqrt{}_{defects} \xrightarrow{\text{further screened by carrier/current injection}}$$

$$\frac{\varepsilon_0 \varepsilon_{dc}}{q} \nabla \square \quad .. \quad \sqrt{}_{defects} \text{-}n(x,j) + p(x,j)$$

From both the current continuity equation and Poisson equation, generally we have

$$j \uparrow, n \uparrow, E \downarrow$$

This is the exactly way how we deal with this. Just as the Poission equation introduced at the beginning:

$$-\nabla \square \left(\frac{\varepsilon \; \varepsilon}{q} \quad \right) = -n + p + N_D(1 - f_D) - N_A f_A + \sum_j N_{tj}(\delta_j - f_{tj}) + N_{it},$$
$$E = -\nabla V$$

It should be emphasized that we make no hypothesis that the polarization charge N_{it} decreases with current injection.

From our previous paper (Z. Gong, et al., Semiconductor Science and Technology, Vol. 27, No. 1, pp. 015003 (2011)), we get a formula between E and *j* as a parabolic fit. The fit is empirical, and may be valid for only certain devices. A standard and self-consistent way is to solve the Poisson equation and current continuity equation.